Electronic Supplementary Material (ESI) for Photochemical & Photobiological Sciences

Supporting Information

to accompany

Generalized solvent scales as a tool for investigating solvent dependence of spectroscopic and kinetic parameters. Application to fluorescent BODIPY dyes

Aleksander Filarowski[‡], Małgorzata Kluba[‡], Katarzyna Cieślik-Boczula[‡], Aleksander Koll[‡], Andrzej Kochel[‡], Lesley Pandey[†], Wim M. De Borggraeve[†], Mark Van der Auweraer[†], Javier Catalán[#] and Noël Boens[†,*]

[‡] *Faculty of Chemistry, University of Wroclaw, F. Joliot-Curie 14, 50-383 Wrocław, Poland*

[†] *Department of Chemistry and Institute for nanoscale Physics and Chemistry (INPAC), Katholieke Universiteit Leuven, Celestijnenlaan 200f – bus 02404, 3001 Leuven, Belgium*

[#] *Departamento de Química Física Aplicada, Universidad Autónoma de Madrid, 28049 Madrid, Spain*

[*] To whom correspondence should be addressed. E-mail: Noel.Boens@chem.kuleuven.be, Fax: +32-16-327990

1. UV–vis absorption and emission spectra of 2

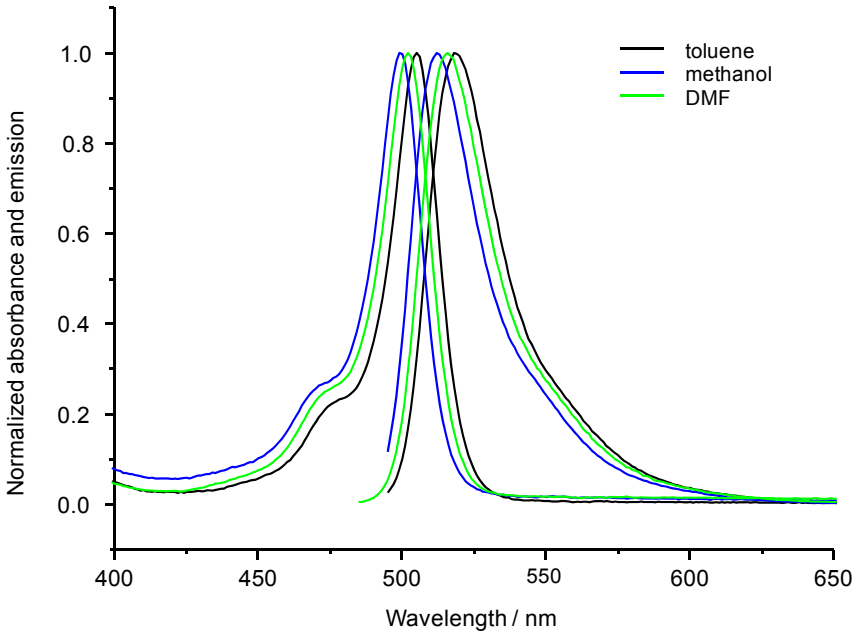

Figure S1. Absorption and fluorescence emission spectra of **2** (at λ_{ex} = 488 nm) in toluene, methanol and DMF normalized to 1.0. Because the spectra all have similar shape and for better clarity, only a limited number of spectra are shown.

2. Solvatochromism

2.1. Compounds 1–3

Solvent-dependent spectral shifts are often interpreted in terms of the Lippert−Mataga equation (eq S1), which describes the solvatochromic Stokes shift $\Delta\bar{\nu}$ (expressed in wavenumbers) as a function of the change of the dipole moment $\Delta\mu_{ge} = \mu_e - \mu_g$ of the dye upon excitation. The validity of eq S1 can be checked by using various solvents with different dielectric constants (ε) and refractive indices (n) and by plotting $\Delta\bar{\nu}$ as a function of $\Delta f = f(\varepsilon) - f(n^2)$.[1, 2]

$$\Delta\bar{\nu} = \frac{2\Delta f}{4\pi\varepsilon_0 hca^3}\left(\mu_e - \mu_g\right)^2 + \text{constant} \qquad \text{(S1a)}$$

$$f(\varepsilon) = (\varepsilon - 1)/(2\varepsilon + 1) \text{ and } f(n^2) = (n^2 - 1)/(2n^2 + 1) \qquad \text{(S1b)}$$

In eq S1, $\Delta\bar{\nu} = \bar{\nu}_{abs} - \bar{\nu}_{em}$ is the solvatochromic shift (in cm^{-1}) between the maxima of absorption and fluorescence emission [$\bar{\nu}_{abs} = 1/\lambda_{abs}(max)$, $\bar{\nu}_{em} = 1/\lambda_{em}(max)$]. h is Planck's constant, c is the velocity of light, ε_0 is the permittivity of vacuum, and a represents the radius of the cavity in which the solute resides. μ_g and μ_e denote the dipole moments of the dye in ground and excited states, respectively.

The use of eq S1 is limited to transitions where the excited state reached after excitation is also the emissive state (hence for $S_0 \rightarrow S_1$ excitation and equal dipole moments for the Franck-Condon and relaxed states) and where the excited-state dipole moment is independent of solvent polarity.

The Lippert–Mataga expression of the Stokes shift (eq S1) depends critically on the change of the solute's dipole moment upon excitation ($\Delta\mu_{ge} = \mu_e - \mu_g$) and the size of the cavity radius (a). The assumptions made in the derivation of the Lippert–Mataga equation (only dipole-dipole interactions are taken into account and the solute polarizability is neglected) together with the uncertainty over the size of the cavity radius explain why the determination of $\Delta\mu_{ge}$ is unreliable.

Figure S2 represents the Lippert−Mataga plot for **1** in the solvents listed in Table 1. As is evident from Figure S2, there is a good linear relationship [correlation coefficient $r = 0.907$, slope = $(7.3 \pm 0.8) \times 10^3$ cm^{-1}, intercept = $(6 \pm 2) \times 10^2$ cm^{-1}] of the Stokes shift $\Delta\bar{\nu}$ versus Δf for the 21 solvents of Table 1. 1,4-Dioxane (#2) is an outlier because its "effective" dielectric constant ε is much higher as it adopts the boat conformation around dipolar species. If one excludes the data point of 1,4-dioxane from of the Lippert–Mataga plot, a better linear regression (not shown in Figure S2) is obtained as assessed by the correlation coefficient ($r = 0.933$).

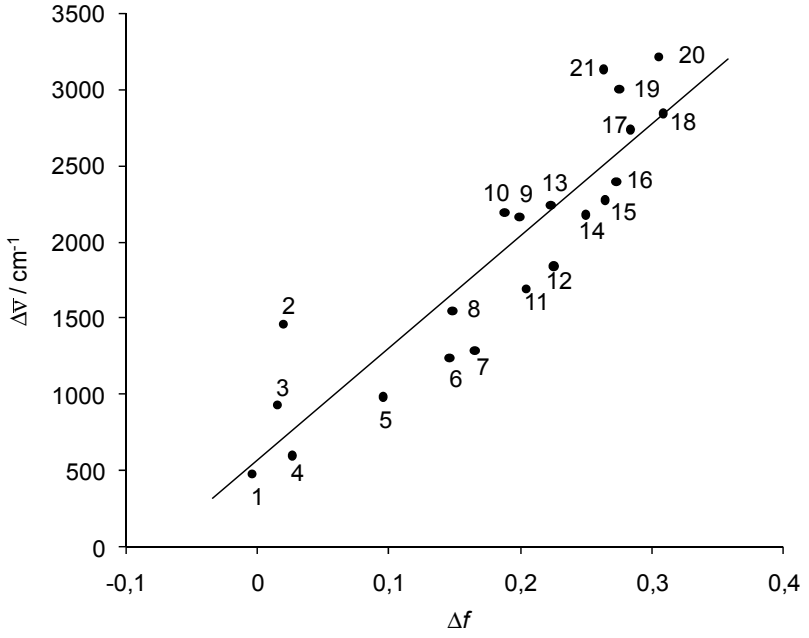

Figure S2. Stokes shift $\Delta\bar{\nu}$ of **1** versus the Lippert solvent parameter $\Delta f = f(\varepsilon) - f(n^2)$. The numbers refer to the solvents in Table 1. The straight line represents the best linear fit to the 21 data points.

Figure S3 represents the Lippert−Mataga plot for **2** in the solvents listed in Table S1. As is evident from Figure S3, the near-independence of the small Stokes shift $\Delta\bar{\nu}$ as a function of Δf – as substantiated by the slight slope [$(1.1 \pm 0.5) \times 10^2$ cm^{-1}] and unsatisfactory correlation coefficient ($r = 0.457$) – indicates that the dye's permanent dipole moments (if any) are similar in the ground and excited states.[1, 2]

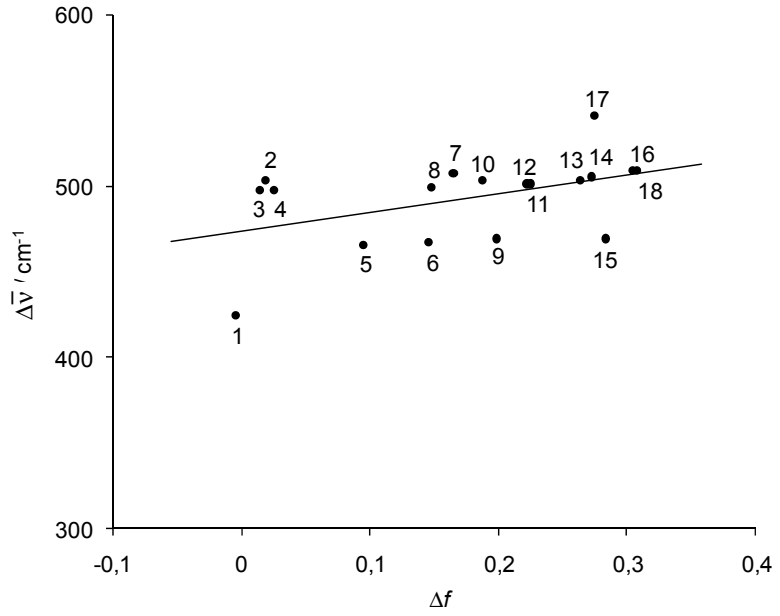

Figure S3. Stokes shift $\Delta\bar{\nu}$ of **2** versus Δf. The numbers refer to the solvents in Table S1. The straight line is the best linear fit to the 18 data points.

Figure S4 shows the Lippert−Mataga plot of **3** for the 14 solvents listed in Table 2. There is a poor linear relationship (correlation coefficient r = 0.697) with a small slope [1.6 ± 0.5) × 10^2 cm^{-1}] between the Stokes shift $\Delta\bar{\nu}$ and Δf.

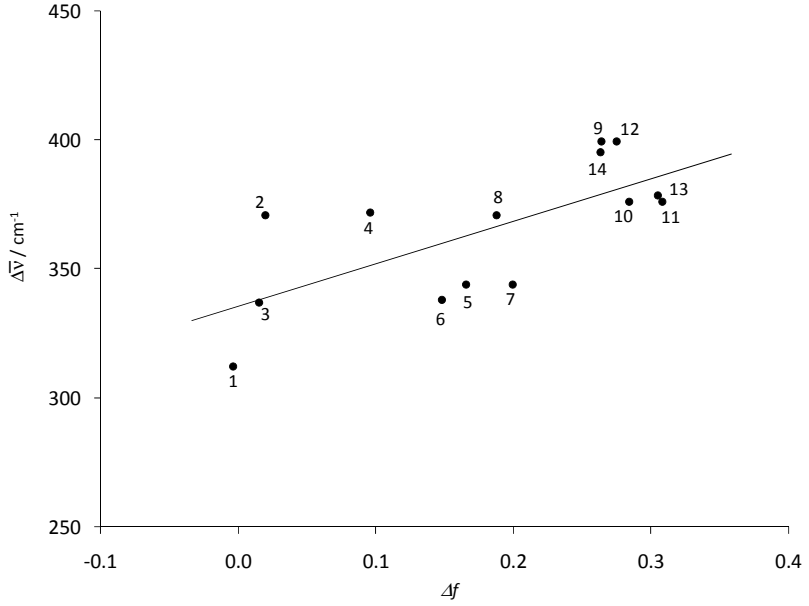

Figure S4. Stokes shift $\Delta\bar{\nu}$ of **3** versus Δf. The numbers refer to the solvents in Table 2. The straight line represents the best linear fit to the 14 data points.

Contrary to the Lippert solvent parameter Δf, other solvent polarity scales – e.g., the normalized $E_T^N(30)$ scale[3] – take into account the hydrogen bond donating and accepting character of the solvent. Figure S5 shows the Stokes shift $\Delta\bar{\nu}$ of **1** as a function of the $E_T^N(30)$ solvent parameter. It is clear that two different sets of solvents can be distinguished: protic and aprotic. There is an adequate linear relationship between the Stokes shift and the $E_T^N(30)$ polarity scale for the aprotic (r = 0.967) and protic (i.e., alcohol) solvents (r = 0.861). A similar linear relationship was found between the fluorescence emission maximum $\bar{\nu}_{em}$ and $E_T^N(30)$ for the aprotic (r = 0.951) and protic (r = 0.783) solvents (figure not shown). For the protic solvents studied (methanol, 2-propanol, 1-butanol, 1-pentanol, 1-octanol), the Stokes shift is much smaller than expected based on the $E_T^N(30)$ scale. This parallels the observations made for the BODIPY analogues with a *p*-aminostyryl subunit at the 3-position[4, 5] and suggests that the contribution of hydrogen bonding to solvation is less important than in the betaine used to construct the $E_T^N(30)$ scale.

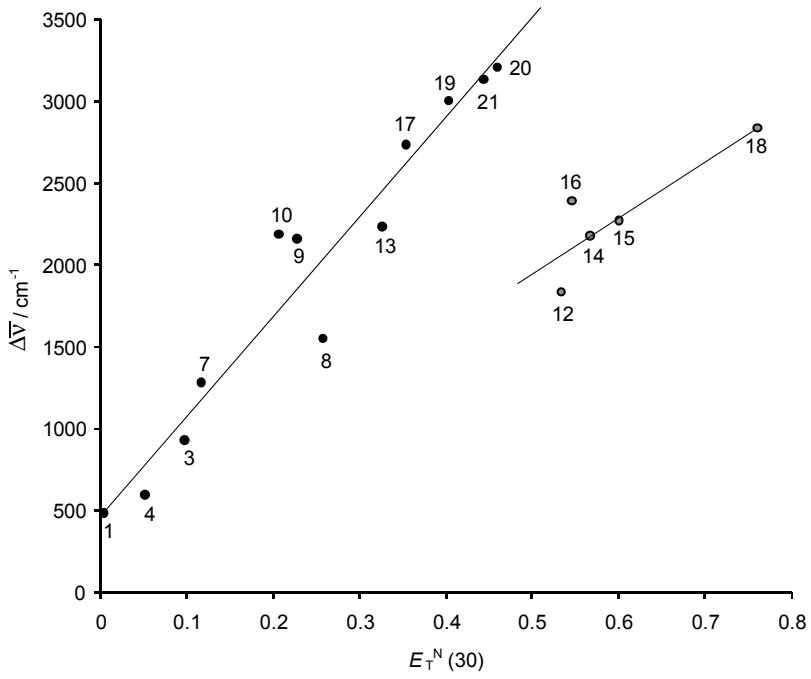

Figure S5. Stokes shift $\Delta\bar{\nu}$ of **1** as a function of the solvent polarity parameter E_T^N (30). The numbers refer to the solvents in Table 1. The straight lines are the best linear fits for the aprotic (filled symbols) and alcohol (grey symbols) solvents.

The solvatochromism of the absorption spectra of **2** can be excellently described by eq 2a, indicating that the small change of $\bar{\nu}_{abs}$ may reflect primarily a slight change in polarizability of the environment of the chromophore. A good linear relationship (eq 2a, r = 0.823) is found between $\bar{\nu}_{abs}$ and SP (Figure S6), with $\bar{\nu}_{abs}^0$ = (20.6 ± 0.1) × 10^3 cm^{-1} and c_{SP} = (–1.0 ± 0.2) × 10^3 cm^{-1}.

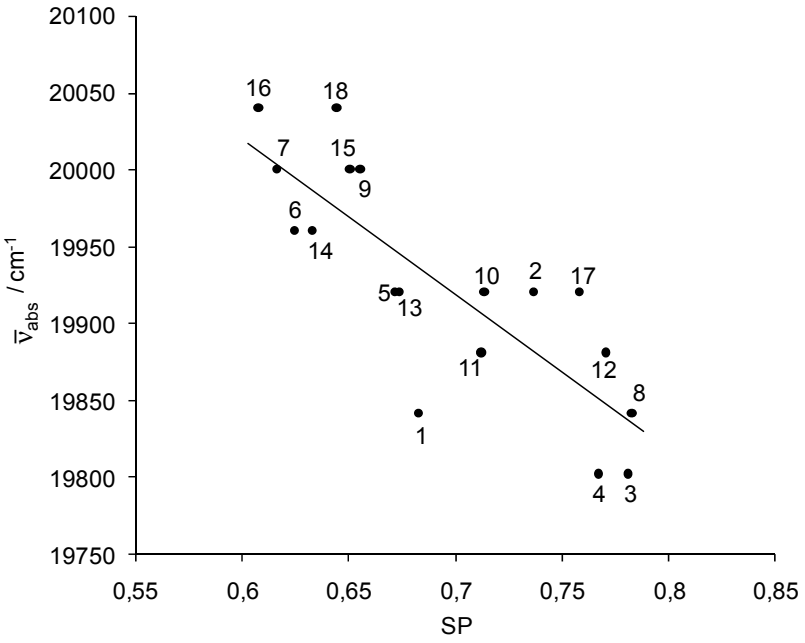

Figure S6. Plot of $\bar{\nu}_{abs}$ of **2** versus the Catalán solvent polarizability parameter SP. The numbers refer to the solvents in Table S1. The straight line is the best linear fit to the data.

The linearity of the plots of the maxima of absorption ($\bar{\nu}_{abs}$, r = 0.907) and fluorescence emission ($\bar{\nu}_{em}$, r = 0.917) of **2** as a function of $f(n^2)$ (Figure S7) corroborates that van der Waals and excitonic interactions with a polarizable solvent can rationalize the solvent dependence of the excitation energy.[6] The slopes of the plots of $\bar{\nu}_{abs}$ [$(-4.1 \pm 0.5) \times 10^3$ cm^{-1}] and $\bar{\nu}_{em}$ [$-(4.3 \pm 0.5) \times 10^3$ cm^{-1}] versus $f(n^2)$ are almost identical.

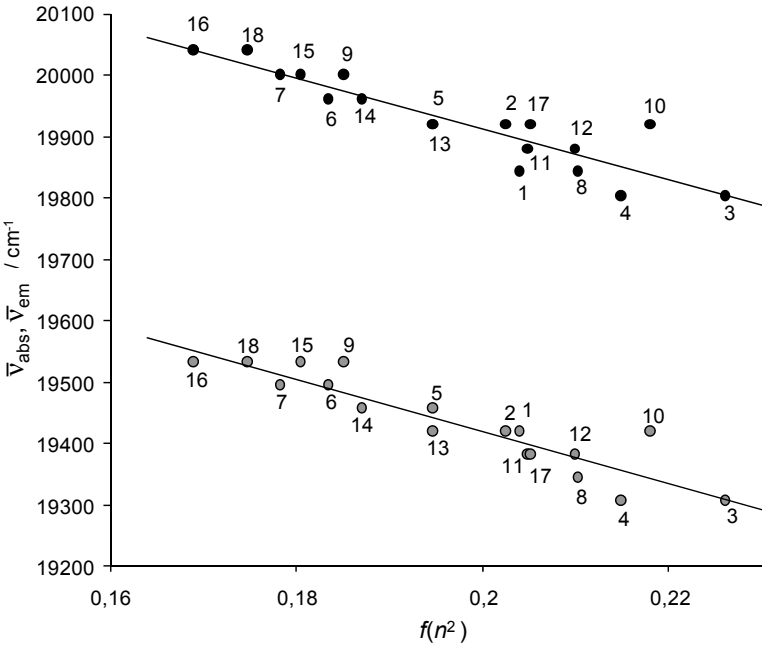

Figure S7. Maxima of the absorption ($\bar{\nu}_{abs}$) and fluorescence emission ($\bar{\nu}_{em}$) for **2** as a function of $f(n^2)$. The numbers refer to the solvents in Table S1. The straight lines represent the best linear fits to $\bar{\nu}_{abs}$ and $\bar{\nu}_{em}$.

To visualize the goodness–of–fit of $\bar{\nu}_{abs}$ of **3** in accordance with the Catalán solvent scales, we present a graph (Figure S8) of the absorption maxima $\bar{\nu}_{abs}$ calculated according to eq 1c using the estimated values of y_0, a_{SA}, b_{SB}, c_{SP} and d_{SdP} versus the corresponding experimental values. As expected, a superb linear relation (r = 0.973) is found between $\bar{\nu}_{abs}$ (exp) and $\bar{\nu}_{abs}$ (calc) with a slope close to one (0.95 ± 0.06).

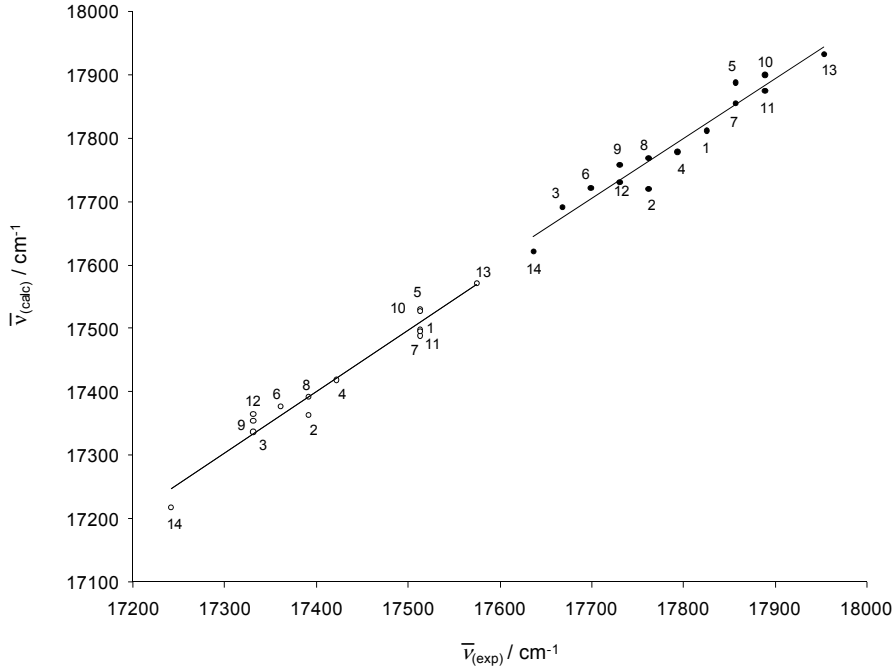

Figure S8. Linear relationship of the experimental and calculated $\bar{\nu}_{abs}$ of **3** (filled symbols) obtained by the multiple linear regression analysis according to eq 1c in which y_0, a_{SA}, b_{SB}, c_{SP} and d_{SdP} are regression coefficients. The straight line is the best linear fit (r = 0.973, slope = 0.95 ± 0.06) to the data. Analogous linear relationship of $\bar{\nu}_{em}$ (calc) versus $\bar{\nu}_{em}$ (exp) of **3** (open symbols). The straight line is the best linear fit (r = 0.980, slope = 0.96 ± 0.06) to the data. The numbers refer to the solvents in Table 2.

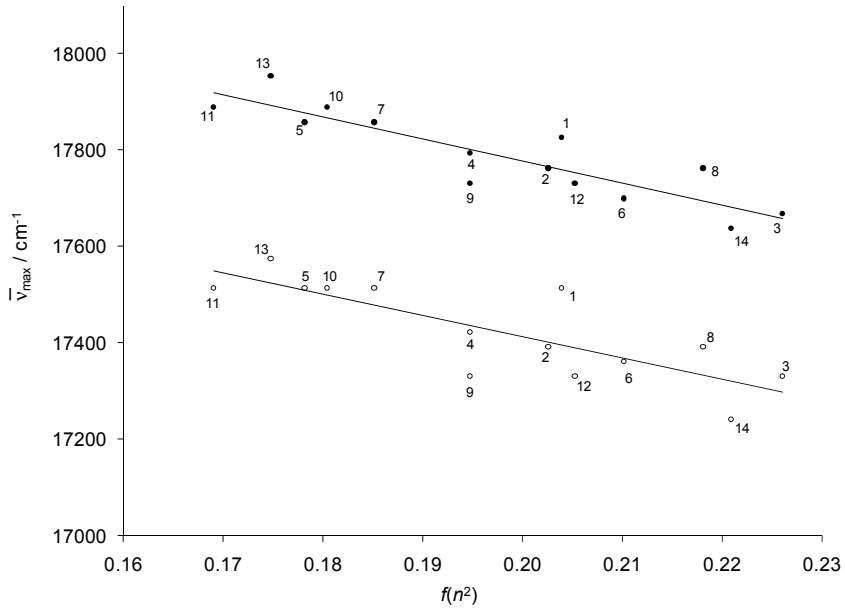

Figure S9. Maxima of the absorption ($\bar{\nu}_{abs}$) and fluorescence emission ($\bar{\nu}_{em}$) of **3** as a function of $f(n^2)$. The numbers refer to the solvents in Table 2. The straight lines represent the best linear fits to $\bar{\nu}_{abs}$ and $\bar{\nu}_{em}$. The slopes of the plots of $\bar{\nu}_{abs}$ versus $f(n^2)$ [(-4.6 ± 0.7) × 10^3 cm^{-1}] and of $\bar{\nu}_{em}$ versus $f(n^2)$ [(-4.4 ± 0.9) × 10^3 cm^{-1}] are very similar.

Table S1. Spectroscopic and photophysical properties of **2** in several solvents.

#	Solvent	λ_{abs}(max) / nm	λ_{em}(max) / nm	$\Delta\bar{\nu}$ / cm^{-1}	$fwhm_{abs}$ / cm^{-1}	Φ_f [a]	τ [b] / ns	k_f / 10^8 s^{-1}	$k_f/\left(n^2\,\bar{\nu}_{em}^3\right)$ / 10^{-5} s^{-1} cm^3	k_{nr} / 10^8 s^{-1}
1	cyclohexane	504	515	424	740	0.34	1.85	1.81	1.22	3.58
2	1,4-dioxane	502	515	503	763	0.31	2.92	1.06	0.72	2.37
3	toluene	505	518	497	767	0.497	2.63	1.90	1.18	1.91
4	tetrachloromethane	505	518	497	741	0.52	2.28	2.28	1.49	2.11
5	dibutyl ether	502	514	465	745	0.30	2.25	1.34	0.93	3.11
6	diisopropyl ether	501	513	467	762	0.33	1.94	1.72	1.24	3.43
7	diethyl ether	500	513	507	745	0.29	2.02	1.42	1.05	3.53
8	chloroform	504	517	499	770	0.46	2.63	1.74	1.15	2.07
9	ethyl acetate	500	512	496	774	0.44	2.32	1.91	1.36	2.40
10	THF	502	515	503	759	0.436	2.32	1.88	1.19	2.43
11	1-octanol	503	516	501	766	0.49	2.66	1.83	1.23	1.93
12	1,2-dichloroethane	503	516	501	782	0.44	2.55	1.73	1.14	2.19
13	1-butanol	502	515	503	782	0.33	3.34	0.99	0.69	2.01
14	2-propanol	501	514	505	770	0.265	2.31	1.15	0.82	3.18
15	acetone	500	512	469	793	0.30	2.10	1.41	1.02	3.36
16	methanol	499	512	509	802	0.29	2.03	1.42	1.08	3.51
17	DMF	502	516	540	816	0.342	2.52	1.36	0.91	2.61
18	acetonitrile	499	512	509	798	0.332	2.18	1.52	1.13	3.06

[a] Φ_f values were determined by excitation at 488 nm. The standard uncertainties on Φ_f are between 0.002 and 0.09.

[b] For the time-resolved fluorescence measurements, the samples were excited at 500 nm. The standard errors on τ are < 10 ps.

2.2. Compounds 4–6 (Figure S10)

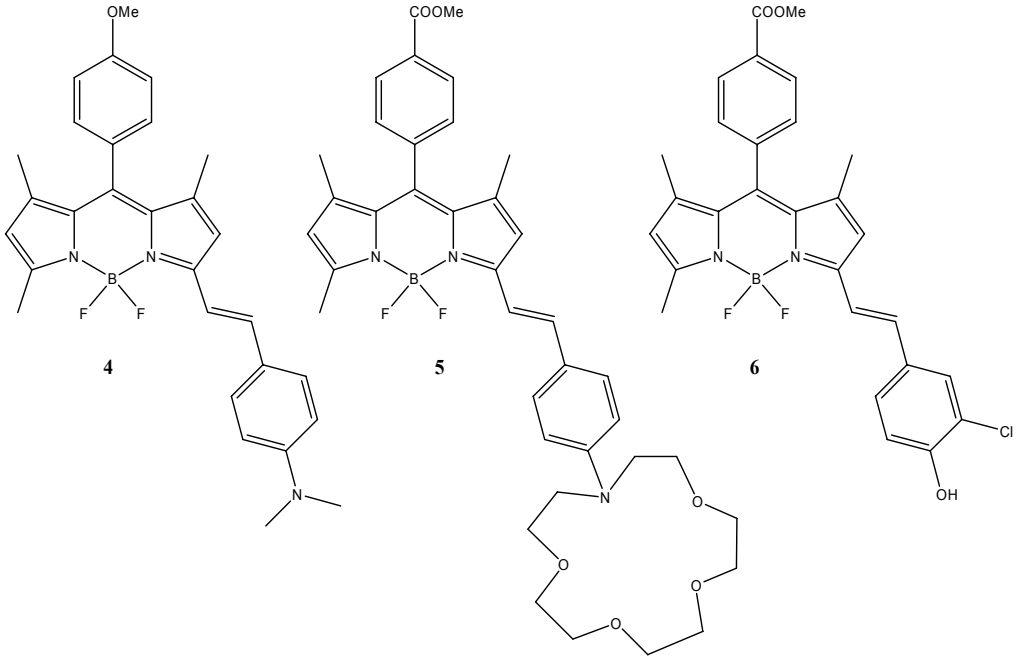

Figure S10. Structure of BODIPY dyes **4**–**6**.

2.2.1. Compound 4

Table S2 lists the y_0, a_{SA}, b_{SB}, c_{SP}, d_{SdP} estimates (eq 1c) and correlation coefficients (r) for the multi-linear regression analyses of $\bar{\nu}_{abs}$, $\bar{\nu}_{em}$ and $\Delta\bar{\nu}$ of **4**, for the 18 pure solvents reported in ref 4.

As found for **1**, $\bar{\nu}_{abs}$ can be perfectly described (r = 0.983) by eq 1c, even though all $\bar{\nu}_{abs}$ values lie within a narrow range (16393–16863 cm^{-1}). The large (negative) estimated c_{SP} coefficient with a relatively small standard error compared to the small estimates of a_{SA}, b_{SB} and d_{SdP} with comparatively large standard errors (Table S2) indicates that the small change of $\bar{\nu}_{abs}$ may be caused mainly by a slight change in solvent polarizability. This is confirmed by the first-rate linear relationship (eq 2a, r = 0.950) between $y = \bar{\nu}_{abs}$ of **4** and SP, with $y_0 = \bar{\nu}^0_{abs} = (18.1 \pm 0.1) \times 10^3$ cm^{-1} and c_{SP} = $(-2.0 \pm 0.2) \times 10^3$ cm^{-1}. Solvent dipolarity is irrelevant for the position of $\bar{\nu}_{abs}$ as is

evident from the comparatively small value of d_{SdP} (Table S2) and is further substantiated by the poor linear fit of $y = \bar{\nu}_{abs}$ as a function of SdP (eq 2b, $r = 0.301$).

The fit of $\bar{\nu}_{em}$ of **4** as a function of the Catalán {SA, SB, SP, SdP} solvent scales also is superb as judged from the high r value (0.981). In agreement with the results for BODIPY analogue **1**, the position of $\bar{\nu}_{em}$ of **4** is determined mainly by solvent dipolarity and not by polarizability. Indeed, the linear fit of $y = \bar{\nu}_{em}$ as a function of SdP (eq 2b, $r = 0.976$) yields $y_0 = \bar{\nu}_{em}^0 = (16.43 \pm 0.09) \times 10^3$ cm^{-1} and $d_{SdP} = (-2.5 \pm 0.1) \times 10^3$ cm^{-1}, while the fit according to eq 2a gives $r = 0.189$. The values of c_{SP} estimated from $\bar{\nu}_{abs}$ and $\bar{\nu}_{em}$ are comparable, taking into account the large standard error on c_{SP} from $\bar{\nu}_{em}$.

The analysis of $\Delta\bar{\nu}$ of **4** according to eq 1c also produces an excellent fit ($r = 0.980$). Here solvent dipolarity is the crucial parameter, as indicated by the high-quality linear fit of $y = \Delta\bar{\nu}$ as a function of SdP (eq 2b, $r = 0.978$), whereas the fit as a function of SP (eq 2a) gives a very low r-value (0.044).

It must be emphasized that the analyses of $\bar{\nu}_{abs}$, $\bar{\nu}_{em}$ and $\Delta\bar{\nu}$ of **4** using the Catalán {SA, SB, SP, SdP} solvent scales are superior to the previously published[4] ones using the Kamlet–Taft {π^*, α, β} and Catalan {SA, SB, SPP} solvent parameters.

Table S2. Estimated coefficients (y_0, a, b, c, d; see eq 1), their standard errors and correlation coefficients (r) for the multiple linear regression analyses of $\bar{\nu}_{abs}$, $\bar{\nu}_{em}$ and $\Delta\bar{\nu}$ of **4**–**6** as a function of the Catalán (eq 1c) solvent scales. 18 Data points were used in the analysis of $\bar{\nu}_{abs}$, $\bar{\nu}_{em}$ and $\Delta\bar{\nu}$ of dyes **4** and **5**. The corresponding number of data points for dye **6** was 12. For the analysis of k_f, $k_f/\left(n^2\,\bar{\nu}_{em}^3\right)$ and k_{nr} 11, 10 and 12 data points for dyes **4**, **5** and **6**, respectively, were used. The regression coefficients are expressed in cm^{-1} for $\bar{\nu}_{abs}$, $\bar{\nu}_{em}$ and $\Delta\bar{\nu}$ and in $10^8\ s^{-1}$ for k_f and k_{nr}.

Dye **4**	y_0	a_{SA}	b_{SB}	c_{SP}	d_{SdP}	r
$\bar{\nu}_{abs}$	$(18.18 \pm 0.08) \times 10^3$	-136 ± 48	-5 ± 33	$(-2.1 \pm 0.1) \times 10^3$	-60 ± 22	0.983
$\bar{\nu}_{em}$	$(17.4 \pm 0.6) \times 10^3$	-31 ± 331	-100 ± 226	$(-1.4 \pm 0.8) \times 10^3$	$(-2.4 \pm 0.2) \times 10^3$	0.981
$\Delta\bar{\nu}$	738 ± 553	-105 ± 323	94 ± 220	-667 ± 778	$(2.4 \pm 0.2) \times 10^3$	0.980
k_f	0.9 ± 1.5	5 ± 7	0.6 ± 0.7	2.9 ± 1.9	-2.2 ± 0.4	0.953
k_{nr}	11 ± 7	10 ± 35	-4 ± 4	-16 ± 10	-6 ± 2	0.888
Dye **5**	y_0	a_{SA}	b_{SB}	c_{SP}	d_{SdP}	r
$\bar{\nu}_{abs}$	$(17.7 \pm 0.1) \times 10^3$	33 ± 55	-83 ± 36	$(-1.9 \pm 0.1) \times 10^3$	-24 ± 28	0.972
$\bar{\nu}_{em}$	$(16.7 \pm 0.4) \times 10^3$	253 ± 240	-399 ± 158	$(-1.1 \pm 0.6) \times 10^3$	$(-2.0 \pm 0.1) \times 10^3$	0.979
$\Delta\bar{\nu}$	920 ± 407	-220 ± 225	316 ± 148	-804 ± 558	$(2.0 \pm 0.1) \times 10^3$	0.982
k_f	0.3 ± 1.1	-0 ± 6	0.4 ± 0.5	2.5 ± 1.5	-1.2 ± 0.4	0.899
k_{nr}	-3 ± 11	18 ± 58	2 ± 5	2 ± 14	6 ± 4	0.810
Dye **6**	y_0	a_{SA}	b_{SB}	c_{SP}	d_{SdP}	r
$\bar{\nu}_{abs}$	$(18.7 \pm 0.1) \times 10^3$	-161 ± 59	-206 ± 48	$(-1.5 \pm 0.1) \times 10^3 \pm$	50 ± 34	0.975
$\bar{\nu}_{em}$	$(18.6 \pm 0.1) \times 10^3$	-285 ± 73	-327 ± 59	$(-1.9 \pm 0.2) \times 10^3 \pm$	-81 ± 42	0.982
$\Delta\bar{\nu}$	79 ± 93	124 ± 54	121 ± 44	308 ± 129	131 ± 31	0.957

2.2.2. Compound 5

Table S2 also collects the estimates y_0, a_{SA}, b_{SB}, c_{SP}, d_{SdP} (eq 1c) and r-values for the multi-linear regression analyses of $\bar{\nu}_{abs}$, $\bar{\nu}_{em}$ and $\Delta\bar{\nu}$ of BODIPY **5** with an aza crown ether functionality for the 18 pure solvents reported in ref 5. As expected, the results of **5** are analogous to those of the BODIPY derivatives **1** and **4** with a *p*-dialkylaminostyryl subunit.

As found for **1** and **4**, $\bar{\nu}_{abs}$ of **5** can be described very well (r = 0.972) by eq 1c, although all $\bar{\nu}_{abs}$ values lie within a narrow range (16051–16501 cm^{-1}). Solvent

polarizability is the main cause for the small variation of $\bar{\nu}_{abs}$. This is demonstrated by the large (negative) c_{SP} estimate with a relatively small standard error in comparison to the small $\{a_{SA}, b_{SB}, d_{SdP}\}$ estimates with comparatively large standard errors (Table S2). Additionally, this is corroborated by the high-quality linear relationship (eq 2a, r = 0.958) between $y = \bar{\nu}_{abs}$ of **5** and SP, with $y_0 = \bar{\nu}^0_{abs} = (17.6 \pm 0.1) \times 10^3$ cm^{-1} and $c_{SP} = (-1.9 \pm 0.1) \times 10^3$ cm^{-1}. That solvent dipolarity is unimportant for the position of $\bar{\nu}_{abs}$ is illustrated by the comparatively small value of d_{SdP} (Table S2) and is confirmed by the poor linear fit of $y = \bar{\nu}_{abs}$ as a function of SdP (eq 2b, r = 0.105).

In agreement with the results of **1** and **4**, the fit of $\bar{\nu}_{em}$ of **5** according to eq 1c is excellent as assessed by its high r-value (0.979). Again, the values of c_{SP} estimated from $\bar{\nu}_{abs}$ and $\bar{\nu}_{em}$ are comparable, taking into account the large standard error on c_{SP} from $\bar{\nu}_{em}$. The change of $\bar{\nu}_{em}$ of **5** is controlled by solvent dipolarity as is evident from the linear fit of $y = \bar{\nu}_{em}$ as a function of SdP (eq 2b, r = 0.962), which yields $y_0 = \bar{\nu}^0_{em} = (15.8 \pm 0.1) \times 10^3$ cm^{-1} and $d_{SdP} = (-2.0 \pm 0.1) \times 10^3$ cm^{-1} which is close to the values found for **1** and **4**. This can explain the large standard error on c_{SP} in the analysis of $\bar{\nu}_{em}$ according to eq 1c with {SA, SB, SP, SdP} as independent variables and the poor fit of $y = \bar{\nu}_{em}$ as a function of SP (eq 2a, r = 0.040).

An excellent fit (r = 0.982) is obtained in the analysis of $\Delta\bar{\nu}$ of **5** according to eq 1c. In accord with the results for **1** and **4**, solvent dipolarity is the crucial parameter influencing the change of $\Delta\bar{\nu}$ of **5**. This can be derived from the first-rate linear fit of $y = \Delta\bar{\nu}$ as a function of SdP (eq 2b, r = 0.973). Solvent polarizability is a negligible parameter, as can be assessed from the analysis of $y = \Delta\bar{\nu}$ as a function of SP (eq 2a, r = 0.147).

As was found for **4**, the regression analyses of $\bar{\nu}_{abs}$, $\bar{\nu}_{em}$ and $\Delta\bar{\nu}$ of **5** using the Catalán {SA, SB, SP, SdP} solvent scales are of better quality than the previously published[5] ones using the Kamlet–Taft {π*, α, β} and Catalan {SA, SB, SPP} solvent parameters.

2.2.3. Compound 6

The estimates y_0, a_{SA}, b_{SB}, c_{SP}, d_{SdP} (eq 1c) and *r*-values for the multi-linear regression analyses of $\bar{\nu}_{abs}$, $\bar{\nu}_{em}$ and $\Delta\bar{\nu}$ of **6** are collected in Table S2 for the 12 solvents reported in ref 7. In agreement with the results obtained for **1**–**5**, perfect fits are obtained for the analysis of $\bar{\nu}_{abs}$, $\bar{\nu}_{em}$ and $\Delta\bar{\nu}$ of **6** as a function of the Catalán {SA, SB, SP, SdP} solvent scales.

The multi-linear analysis of the $\bar{\nu}_{abs}$ data according to eq 1c gives an excellent fit (r = 0.975). It is remarkable that the small solvatochromic shifts $\bar{\nu}_{abs}$ of **6** (17361–17730 cm^{-1}) can be described so accurately by the Catalán {SA, SB, SP, SdP} solvent scales. That solvent polarizability is the most critical factor influencing the slight change of $\bar{\nu}_{abs}$ is derived from the high-quality linear relationship (eq 2a, r = 0.830) between y = $\bar{\nu}_{abs}$ of **6** and SP, with $y_0 = \bar{\nu}^0_{abs} = (18.4 \pm 0.2) \times 10^3$ cm^{-1} and $c_{SP} = (-1.3 \pm 0.3) \times 10^3$ cm^{-1}. Solvent dipolarity is largely unimportant for the position of $\bar{\nu}_{abs}$, as derived from the inadequate linear fit of $\bar{\nu}_{abs}$ as a function of SdP (eq 2b, r = 0.166).

The solvatochromic shifts of $\bar{\nu}_{em}$ of **6** can be described outstandingly well (r = 0.982) by eq 1c. The large (negative) c_{SP} estimate with a relatively small standard error (Table S2) suggests that $\bar{\nu}_{em}$ is mainly influenced by a change in solvent polarizability. This is corroborated by the three analyses of $\bar{\nu}_{em}$ according to eq 1c with {SA, SB, SP}, {SB, SP, SdP} and {SA, SP, SdP} as independent variables,

which all give high-quality fits with r = 0.972, 0.940 and 0.896, respectively. The common independent variable in these analyses is SP. Conversely, the analysis of $\bar{\nu}_{em}$ according to eq 1c, in which solvent polarizability is disregarded, gives a low r-value (0.608). These analyses signify that solvent polarizability is the most crucial solvent property affecting $\bar{\nu}_{em}$. As observed for all other compounds, c_{SP} estimated from $\bar{\nu}_{em}$ data equals, within experimental error, c_{SP} obtained from $\bar{\nu}_{abs}$ data.

An excellent fit (r = 0.957) is obtained in the analysis of $\Delta\bar{\nu}$ of **6** according to eq 1c. As before, solvent dipolarity is the most important parameter influencing the change of $\Delta\bar{\nu}$ of **6**. This can be derived from the good linear fit of $y = \Delta\bar{\nu}$ as a function of SdP (eq 2b, r = 0.840). Solvent polarizability is unimportant, as can be derived from the analysis of $y = \Delta\bar{\nu}$ as a function of SP (eq 2a, r = 0.106).

3. Time-resolved fluorescence of 4–6

3.1. Compound 4

The estimates y_0, a_{SA}, b_{SB}, c_{SP}, d_{SdP} (eq 1c) and r-values for the multi-linear regression analyses of k_f and k_{nr} of **4** are collected in Table S2 for the 11 data points available in ref 4.

Analysis of k_f of **4** according to eq 1c gives an excellent fit, as judged by its r-value (0.953, Table S2). The important factor influencing k_f is solvent (di)polarity. Indeed, there is an excellent linear relation (r = 0.932) between $y = k_f$ and SdP (eq 2b), with $y_0 = k_f^0 = (3.1 \pm 0.2) \times 10^8$ s^{-1} and $d_{SdP} = (-2.1 \pm 0.3) \times 10^8$ s^{-1}. The linear fit of $y = k_f$ as a function of SP (eq 2a, r = 0.461) indicates that solvent polarizability is much less decisive for the change of k_f.

The multi-linear Catalán fit of $y = k_f/\left(n^2\,\bar{\nu}_{em}^3\right)$ yields an *r*-value of 0.867, indicating that the transition dipole moment $\langle \psi_G | \hat{\mu} | \psi_E \rangle$ depends on the solvent.

The multi-linear analysis of k_{nr} according to eq 1c gives an excellent fit, as assessed by the high *r*-value (0.888). The important factor influencing k_{nr} is again solvent (di)polarity as derived from the good linear fit ($r = 0.809$) of k_{nr} as a function of SdP (eq 2b). The analysis of $y = k_{nr}$ as a function of SP (eq 2a, $r = 0.422$) signifies that solvent polarizability is much less important for the change of k_{nr}.

3.2. Compound 5

The estimates y_0, a_{SA}, b_{SB}, c_{SP}, d_{SdP} (eq 1c) and *r*-values for the multi-linear regression analyses of k_f and k_{nr} of **5** are collected in Table S2 for the 10 data points available in ref 5.

Analysis of k_f of **5** according to eq 1c gives a good fit, as assessed by its *r*-value (0.899, Table S2). The important factor influencing k_f is solvent (di)polarity: the linear regression of $y = k_f$ versus SdP (eq 2b, $r = 0.834$) yields $y_0 = k_f^0 = (2.2 \pm 0.1) \times 10^8\ s^{-1}$ and $d_{SdP} = (-1.0 \pm 0.2) \times 10^8\ s^{-1}$. Solvent polarizability is not important for the change of k_f: the linear fit of $y = k_f$ as a function of SP (eq 2a) has an *r*-value of only 0.235.

The multi-linear Catalán analysis of $y = k_f/\left(n^2\,\bar{\nu}_{em}^3\right)$ according to eq 1c yields an *r*-value of 0.666, implying that there is no clear correlation between $k_f/\left(n^2\,\bar{\nu}_{em}^3\right)$ and the {SA, SB, SP, SdP} parameters and demonstrates that the transition dipole moment $\langle \psi_G | \hat{\mu} | \psi_E \rangle$ stays practically constant even in solvents of high polarity ($\varepsilon = 36.7$ for DMF). The average value of $k_f/\left(n^2\,\bar{\nu}_{em}^3\right)$ for the 10 data points available from ref 5 is $(2.5 \pm 0.3) \times 10^{-5}\ s^{-1}\ cm^3$.

The multi-linear analysis of k_{nr} according to eq 1c gives an acceptable fit, as assessed by its *r*-value (0.810). The important factor influencing k_{nr} is solvent (di)polarity as derived from the good linear fit (r = 0.803) of k_{nr} as a function of SdP (eq 2b). The analysis of $y = k_{nr}$ as a function of SP (eq 2a, r = 0.070) entails that solvent polarizability is not important for the variation of k_{nr}.

3.3. Compound 6

Here we analyze the 12 k_f and $k_f/\left(n^2\,\bar{\nu}_{em}^3\right)$ data available from ref 7 for BODIPY **6**. Reliable data analyses of the k_{nr} values could not be obtained because six Φ_f values are equal to 1.00 (yielding $k_{nr} = 0\ s^{-1}$), while the remaining six Φ_f are between 0.93–0.98. Six data points is not enough for a reliable multi-linear analysis according to eq 1c.

There is no a clear dependency of k_f on the Catalán {SA, SB, SP, SdP} solvent scales, as derived from the *r*-value (0.706). The radiative rate constant k_f averaged over the 12 solvents reported in ref 7 is $(2.6 \pm 0.2) \times 10^8\ s^{-1}$. The inadequate correlation between $k_f/\left(n^2\,\bar{\nu}_{em}^3\right)$ and the {SA, SB, SP, SdP} parameters (r = 0.758) indicates that the transition dipole moment $\langle \psi_G | \hat{\mu} | \psi_E \rangle$ is invariant, even in solvents of high (di)polarity (ε = 46.7 for DMSO). The mean $k_f/\left(n^2\,\bar{\nu}_{em}^3\right)$ value calculated for the 12 data points available from ref 7 is $(2.6 \pm 0.1) \times 10^{-5}\ s^{-1}\ cm^3$.

4. Synthesis of 1 and 3

4,4-difluoro-3-{2-[4-(dimethylamino)phenyl]ethenyl}-8-[4-(methoxycarbonyl) phenyl]-1,5,7-trimethyl-3a,4a-diaza-4-bora-*s*-indacene (1), (Scheme 1). Compound **2** (584.8 mg, 1.5 mmol), *p*-*N*,*N*-dimethylaminobenzaldehyde (270 mg, 2 mmol), piperidine (0.1 mL, 1 mmol), acetic acid (0.1 mL, 1.2 mmol) and a small amount of

molecular sieves were suspended in dry toluene in a 15 mL glass tube sealed with a teflon cap. The sample was irradiated at 200 W and 190 °C for 20 min in a CEM-Discover monomode microwave apparatus. After completion of the reaction, the cooled mixture was poured directly onto a silica column and eluted with dichloromethane. The collected pink fraction was concentrated under vacuum and dried to obtain 181.3 mg (31% yield) of compound **1**. Mp > 300 °C. ^{13}C NMR (1,1,2,2-tetrachloroethane-d_2) δ 166.5 ($\underline{C}O_2CH_3$), 155.1, 153.0, 151.0, 142.8, 140.5, 139.9, 138.4, 137.2, 132.5, 130.4, 130.2, 129.3, 128.6, 124.1, 120.7, 118.0, 113.8, 111.9, 52.4 (OCH_3), 40.1($N(CH_3)_2$), 14.8, 14.6, 14.3. ^{1}H NMR, 600MHz, (1,1,2,2-tetrachloroethane-d_2), δ 8.19 [d, 2 H, J = 8.1 Hz], 7.52 [d, 2 H, J = 8.1 Hz], 7.46 [d, 2 H, J = 8.4 Hz], 7.41 [d, 1 H, J = 15.3 Hz], 7.24 [d, 1 H, J = 16.4 Hz], 6.71 [d, 2 H, J = 8.42 Hz], 6.64 [s, 1 H], 6.02 [s, 1 H], 3.97 [s, 3 H, OCH_3], 3.04 [s, 6 H, $N(CH_3)_2$], 2.58 [s, 3 H], 1.42 [s, 3 H], 1.38 [s, 3 H]. LRMS *m/z* 513 (M^+ 100). HRMS: calcd for $C_{30}H_{30}BF_2N_3O_2$ 513.2399, found 513.2409.

4,4-difluoro-3-[2-(4-fluoro-3-hydroxyphenyl)ethenyl]-8-[4-(methoxycarbonyl) phenyl]-1,5,7-trimethyl-3a,4a-diaza-4-bora-*s*-indacene (3), (Scheme 1). Compound **2** (13.5 mg, 0.035 mmol), 4-fluoro-3-hydroxybenzaldehyde (4.2 mg, 0.03 mmol), piperidine (0.1 mL), acetic acid (0.1 mL) and a small amount of molecular sieves were suspended in 2 mL of dry toluene in a 10 mL glass tube sealed with a teflon cap. The sample was irradiated at 200 W and 190 °C for 20 min in a CEM-Discover monomode microwave apparatus. After completion of the reaction, the cooled mixture was poured directly onto a silica column and eluted with dichloromethane to yield 5.2 mg (34% yield) of purple crystals of **3**. mp 224 °C.

^{1}H NMR (300 MHz, $CDCl_3$) 8.19 (d, 2H, J = 8 Hz, Ar-H), 7.56 (d, 1H, J = 16.5 Hz, vinyl-H), 7.43 (d, 2H, J = 8 Hz, Ar-H), 7.27 (br m, 1H overlap with residual $CHCl_3$),

7.18 (d, 1H, *J* = 16.5 Hz, vinyl-H), 7.09-7.05 (m, 2H, Ar-H), 6.58 (s, 1H), 6.03 (s, 1H), 5.42 (br s, 1H, OH), 3.97 (s, 3H, OCH3), 2.60 (s, 3H), 1.41 (s, 3H), 1.38 (s, 3H). HRMS (EI) calcd for $C_{28}H_{24}BF_3N_2O_3$ 504.1832, found 504.1832

^{1}H and ^{13}C NMR spectra of **1** and **2** were recorded at room temperature on a Bruker Avance II 600 spectrometer operating at 600 MHz for ^{1}H and 150 MHz for ^{13}C. ^{1}H NMR spectra were recorded in 1,1,2,2-tetrachloroethane-d_2 and referenced to the solvent peak thereof (6.00 ppm). Chemical shift multiplicities are reported as s = singlet and d = doublet. ^{13}C spectra were referenced to the 1,1,2,2-tetrachloroethane-d_2 signal (73.78 ppm).

^{1}H and ^{13}C NMR spectra of **3** were recorded on a Bruker Avance 300 operating at a frequency of 300 MHz for ^{1}H and 75 MHz for ^{13}C. ^{1}H NMR spectra were referenced to tetramethylsilane (0.00 ppm) as an internal standard. Chemical shift multiplicities are reported as s = singlet, d = doublet and m = multiplet. ^{13}C spectra were referenced to the $CDCl_3$ (77.67 ppm) signal.

Mass spectra were recorded on a Thermo Electron LCQ Advantage mass spectrometer (ESI+ mode). High resolution mass data were obtained with a KRATOS MS50TC instrument. Melting points were taken on a Reichert Thermovar and are uncorrected.

References and Notes

(1) E. Lippert, Dipolmoment und Elektronenstruktur von angeregten Molekülen, Z. *Naturforsch., A: Phys. Sci.* **1955**, *10*, 541−545.

(2) (a) N. Mataga, Y. Kaifu and M. Koizumi, The solvent effect on fluorescence spectrum – change of solute-solvent interaction during the lifetime of excited solute molecule, *Bull. Chem. Soc. Jpn.* **1955**, *28*, 690−691. (b) N. Mataga, Y. Kaifu and M. Koizumi, Solvent effects upon fluorescence spectra and the dipole moments of excited molecules, *Bull. Chem. Soc. Jpn.* **1956**, *29*, 465−470.

(3) C. Reichardt, Solvatochromic dyes as solvent polarity indicators, *Chem. Rev*. **1994**, *94*, 2319−2358.

(4) M. Baruah, W. Qin, C. Flors, J. Hofkens, R. A. L. Vallée, D. Beljonne, M. Van der Auweraer, W. M. De Borggraeve and N. Boens, Solvent and pH dependent fluorescent properties of a dimethylaminostyryl borondipyrromethene dye in solution, *J. Phys. Chem. A* **2006***, 110*, 5998−6009.

(5) W. Qin, M. Baruah, M. Sliwa, M. Van der Auweraer, W. M. De Borggraeve, D. Beljonne, B. Van Averbeke and N. Boens, Ratiometric, fluorescent BODIPY dye with aza crown ether functionality: synthesis, solvatochromism, and metal ion complex formation, *J. Phys. Chem. A* **2008***, 112*, 6104−6114.

(6) D. Pevenage, D. Corens, W. Dehaen, M. Van der Auweraer, F. C. De Schryver, Influence of the N-substituent on the photophysical properties of oxacarbocyanines in solution, *Bull. Soc. Chim. Belg*. **1997**, *106*, 565–572.

(7) W. Qin, M. Baruah, W. M. De Borggraeve and N. Boens, Photophysical properties of an on/off fluorescent pH indicator excitable with visisble light based in a borondipyrromethene-linked phenol, *J. Photochem. Photobiol. A: Chem.* **2006**, *183*, 190−197.